Testing of Folding Wing-Tip for Gust Load Alleviation in High Aspect Ratio Wing

R.C.M. Cheung[1], D. Rezgui[2] and J.E. Cooper[3]
Department of Aerospace Engineering, University of Bristol, University Walk, Bristol, BS8 1TH, UK.

and
T. Wilson[4]
Airbus Operations Ltd, Filton, Bristol, BS34 7PA, UK.

Folding wing-tips have begun to feature on recent aircraft designs, as a solution for compliance with existing airport gate width, whilst the higher aspect ratio will lead to lower induced drag and better overall fuel efficiency. Recent studies have suggested that by allowing folding of the wing-tip during flight, additional gust load alleviation can be achieved. This paper describes the follow-on work from a previous experimental study, in which the folding wing-tip concept is now applied to a new wind tunnel model of a high aspect ratio wing with a much-reduced bending stiffness. Using a low-speed wind tunnel with a vertical gust generator, the experiment examined the load alleviation performance through a range of one-minus-cosine gust inputs and found up to 11% reduction in peak wing-root bending moment. In addition, a movable secondary aerodynamic surface was fitted to the folding wing-tip which demonstrated that such a device was able to control the orientation of the folding wing-tip effectively in steady aerodynamic conditions, as well as achieving further reduction in peak wing-root bending moment during gust encounters through active control.

Nomenclature

Symbols

α	=	Angle of attack
δ	=	Angular deflection of the secondary aerodynamic surface
γ	=	Hinge angle
Λ	=	Sweep angle
θ	=	Fold angle of the wing-tip
ζ	=	Servo demand parameter
f	=	Frequency
g	=	Acceleration due to gravity
m	=	Mass
t	=	Time
x	=	Distance
v	=	Wind tunnel velocity
C_L	=	Lift coefficient

I. Introduction

An increasing number of aircraft designs have focused on using high aspect ratio wings for better aerodynamic efficiency. Whilst lower induced drag can reduce the fuel required or increase the range of the aircraft, the increased structural weight due the larger wingspan can limit the overall gain. A longer wingspan could also lead to operational

[1] Research Associate, Department of Aerospace Engineering.
[2] Lecturer in Aerospace Engineering, Department of Aerospace Engineering.
[3] Airbus Royal Academy of Engineering Sir George White Professor of Aerospace Engineering, FAIAA.
[4] Loads and Aeroelastics, Flight Physics Department.

difficulties as existing airport gates may be too narrow. The latest B-777 aircraft overcomes this problem by incorporating a mechanism to fold up its wing-tips as it taxies to the airport gate[1].

The inclusion of folding wing-tips in modern airliners also opens up the possibility of utilizing them as a new type of gust load alleviation device. Since aircraft structures are sized based upon the critical load cases from gusts and maneuvers, a reduction in the magnitude of these loads can result in lower aircraft weight. Therefore, effective gust load alleviation can lead to more light-weight, fuel-efficient and environmentally friendly aircraft. In fact, a number of modern jet aircraft already employ active gust load alleviation systems whereby the motion due to the unsteadiness of oncoming air is sensed by accelerometers and then control laws are used to activate the ailerons to reduce the loads and motions that are experienced by the aircraft[2]. By contrast, a folding wing-tip could function as a passive gust load alleviation device, if an appropriate hinge geometry is utilized. This benefit originates from the geometric relationship between the orientation of the wing-tip folding axis and the change in the effective local angle of attack of the wing-tip as it folds, which is described by

$$\Delta\alpha_{WT} = -\tan^{-1}(\tan\theta \sin\gamma) \tag{1}$$

where the hinge angle γ denotes the orientation of the folding axis from the longitudinal axis of the aircraft and the fold angle θ refers to the angular displacement of the wing-tip from the wing-level position, as shown in Figure 1 and Figure 2 respectively.

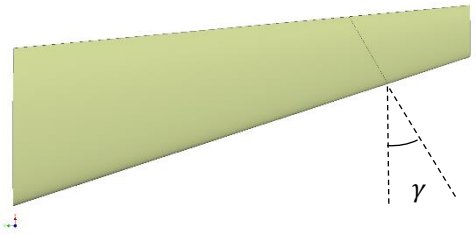

Figure 1 Hinge angle γ.

Figure 2 Fold angle θ.

Consequently, the zero-value hinge angle shown in Figure 3 provides no additional gust alleviation capability, as the local angle of attack of the wing-tip is unchanged. However, when the folding hinge is configured with a positive hinge angle as shown in Figure 4, the local angle of attack of the wing-tip decreases with the folding action, which can reduce its bending moment contribution during a vertical gust encounter and thus achieving gust load alleviation.

Figure 3 0 deg hinge angle.

Figure 4 30 deg hinge angle.

A previous study[3] investigating non-zero-value hinge angle configurations and variation in the folding hinge stiffness demonstrated that the peak wing root bending moment could be reduced by allowing the wing-tip to fold during gust encounters. This finding agrees with several other studies[4-6] that also utilized simple passive means for controlling the folding motion. All these studies found that low hinge stiffness in their respective passive system gave a good level of gust load alleviation performance, however further gains could be obtained if the responsiveness of the folding action could be improved. More complex solutions have been proposed to address this issue, including the use of nonlinear spring systems[7, 8] and bi-stable constructs[9] to provide the required hinge stiffness properties. These approaches focus on their inherent snap-through action to help speed up the folding motion, while retaining some effective hinge stiffness for aero-static positioning of the wing-tip. A natural extension of these concepts is to combine the passive folding wing-tip with an active secondary aerodynamic surface to achieve the same function.

The work described in this paper extends from the previous experimental study by the authors[3], in which a gust load alleviation capability was demonstrated using a low aspect ratio wing. The current work focuses on the application of the folding wing-tip concept to a more flexible high aspect ratio wing, of which the dynamic effect of

wing bending is more dominate. Low-speed wind tunnel testing is carried out to investigate the effect of a non-zero hinge angle has on the interaction between the wing-tip and wing, and the overall gust load alleviation performance. In addition, this work also explores the effectiveness of using an actively controlled secondary aerodynamic surface in the folding wing-tip to enhance the control over the orientation of the wing-tip in steady conditions, as well as assesses the feasibility of using such a system to achieve better performance over a simple passive folding wing-tip.

II. Wind Tunnel Model

A. Design

The current work primarily aims to improve the understanding of how the folding wing-tip concept may be applied to a flexible high aspect ratio wing for reducing the peaking loading during a gust encounter. For this reason, the current wind tunnel model has a semi-span of 1.345m, with a constant chord length of 0.150m. The equivalent full-wing aspect ratio is 18.7, which is a significant increase from the aspect ratio of 6.7 used in the previous study. The same constant sectional profile of NACA0015 has been retained for consistency and internal clearance for sensors and servo cable routing. Unlike the previous model, the section inboard of the folding hinge is considerably more flexible in bending. Structural stiffness of this section is provided by a 316L stainless steel beam that spans from the wing-root to the folding hinge section, covered by several skin panels for the required aerodynamic profile. As shown in Figure 5(a), these skin panels are intentionally spaced apart to avoid touching even when the magnitude of wing bending is large, such that the overall bending and torsional stiffness of the wing remain similar to that of the underlying beam.

The higher flexibility in the wing structure dictates that the variable sweep approach from the previous design cannot be used to change the effective hinge angle without risking its effect being reduced by the natural bend-twist coupling of a flexible swept wing. Therefore, the wind tunnel model for this study is un-swept with the wing-tip folding hinge located at 1.000m from the wing-root and oriented at a hinge angle of 10.0 deg. In this arrangement, the folding wing-tip constitutes 29% of the total wetted area of the entire wing.

As shown in Figure 5(a) and (b), a movable secondary aerodynamic surface, referred to as the wing-tip tab, is featured on the folding wing-tip at the 75% chord position. The wing-tip tab has a span of 0.100m and it is driven directly by a Maxon EC-i30 brushless motor for active control.

B. Instrumentation

The wind tunnel model is equipped with an RLS RM08 magnetic encoder at the folding hinge for measuring the fold angle of the wing-tip. There is a total of six accelerometers installed in the wind tunnel model, consisting of an Endevco Model 65L, a PCB Piezotronics 356A32, a PCB Piezotronics 352C65 and three PCB Piezotronics M352C65. Four accelerometers are installed in pairs at two spanwise stations inboard of the folding hinge, at 0.295m and 0.820m. The remaining accelerometers are located near the tip of the wing-tip at 1.337m. Four Vishay Micro-measurements CEA-09-125UN strain gages in full-bridge configuration are installed on the main beam to provide wing-root bending moment measurement. The total load on the wind tunnel model was measured using a custom-built balance equipped with an AMTI MC3A-1000 and an AMTI MC3A-250 load cell. An iMetrum ICA-3D-1000-03 camera system was used to monitor deflection of the wind tunnel model under load. The accelerometers and the encoder were connected to a National Instruments cDAQ-9172 chassis, equipped with a NI-9205, a NI-9263 and three NI-9234 modules. The strain gages were connected a PXIe-4330 card hosted by a National Instruments PXIe-1082 chassis. Matlab was used for data acquisition, in which the deflection demand signal for the wing-tip tab was generated and synchronized using the same software platform.

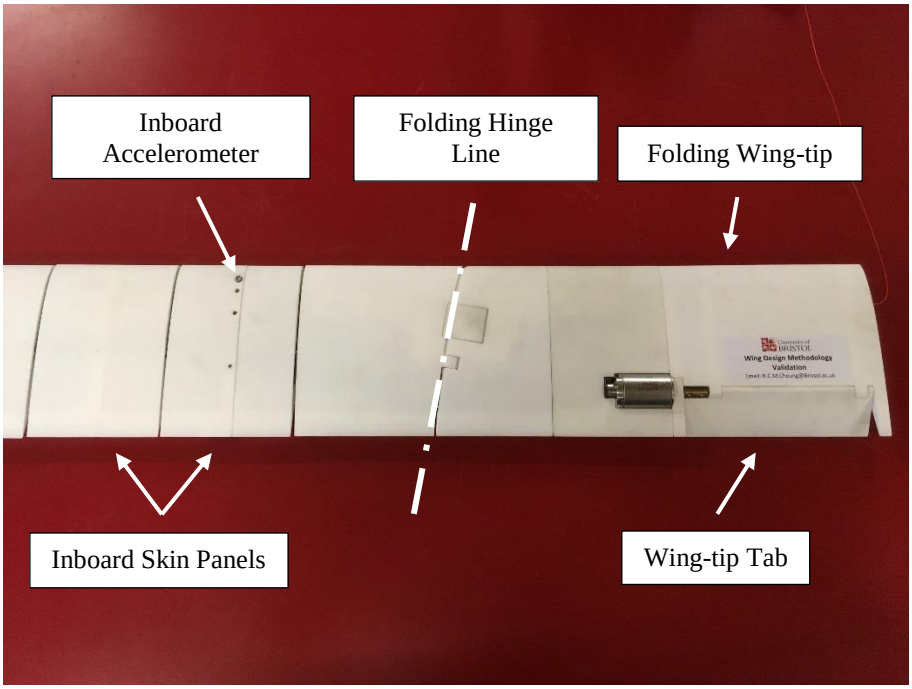

(a) Folding hinge section.

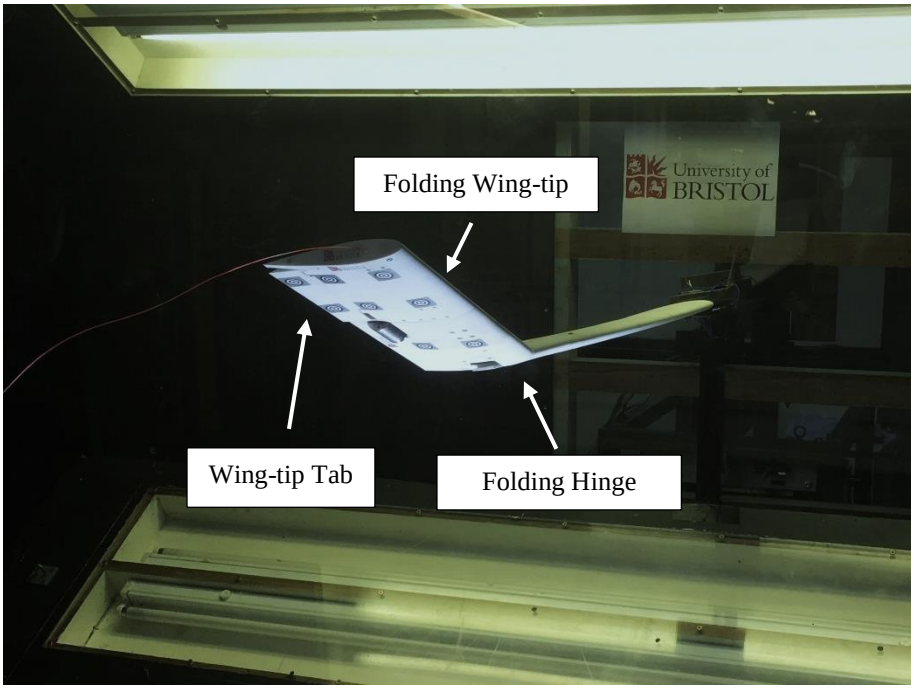

(b) Free-hinge configuration.

Figure 5 Wind tunnel model.

C. Testing

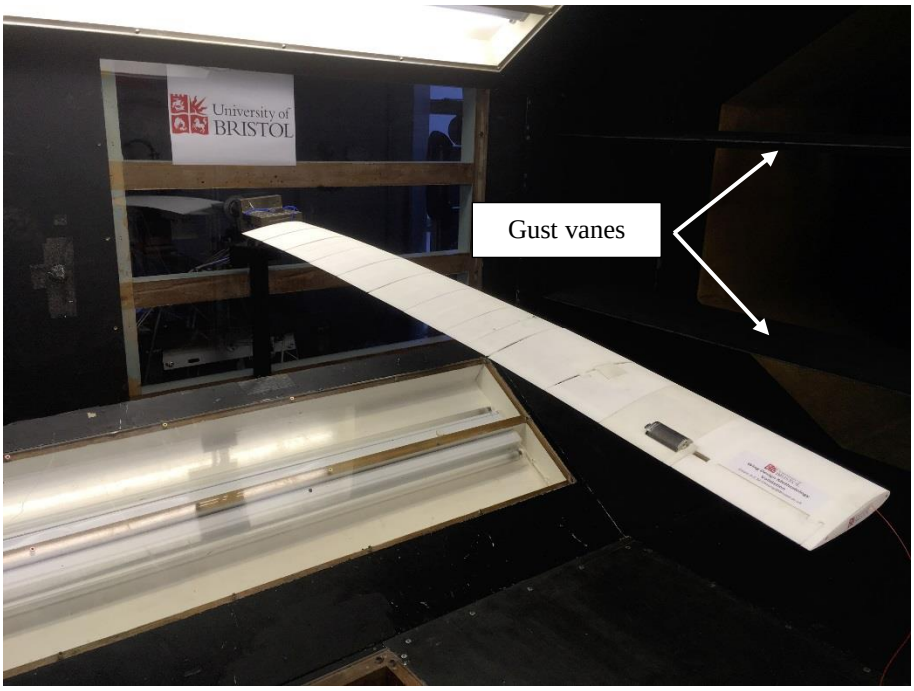

Figure 6 Working section of the 7ft by 5ft wind tunnel at the University of Bristol.

Testing was carried out in the 7ft by 5ft low-speed closed-return wind tunnel at the University of Bristol, which is equipped with a dual-vane vertical gust generator[10] as shown in Figure 6. The test campaign comprised of three phases. In the first phase of testing, the wind tunnel model was tested in steady aerodynamic conditions to establish the aero-static behavior of the folding wing-tip and the characteristics of the wing-tip tab as a trimming device for wing-tip fold angle. In the second phase of the test campaign, the wind tunnel model was subjected to one-minus-cosine gust excitations of various gust lengths to evaluate the gust load alleviation performance of the folding wing-tip concept. The third phase of testing explored using the wing-tip tab through open-loop control during a gust to further enhance the overall gust load alleviation. The wind tunnel model was nominally set to a configuration in which the wing-tip could freely rotate about the folding hinge. When appropriate, a baseline reference was obtained by locking the wing-tip in the wing-level orientation. These two configurations of the wing-tip are referred to as the free-hinge and the locked-hinge configuration.

III. Results

A. Steady conditions

Figure 7 shows a comparison of the measured lift between the free-hinge configuration and the locked-hinge reference in steady aerodynamic conditions with zero wing-tip tab deflection. In both configurations, the lift-curve exhibits linearity at lower angles of attack, but its gradient reduces at higher angles of attack. As a reference, each lift-curve is linearized in the low angle of attack region, with the resulting coefficients listed in Table 1.

Table 1. Linearized lift-curve at low angles of attack.

Configuration	C_{L_α}, rad^{-1}	α_0, rad
Locked-hinge	5.5708	-0.0328
Free-hinge	5.4096	-0.0553

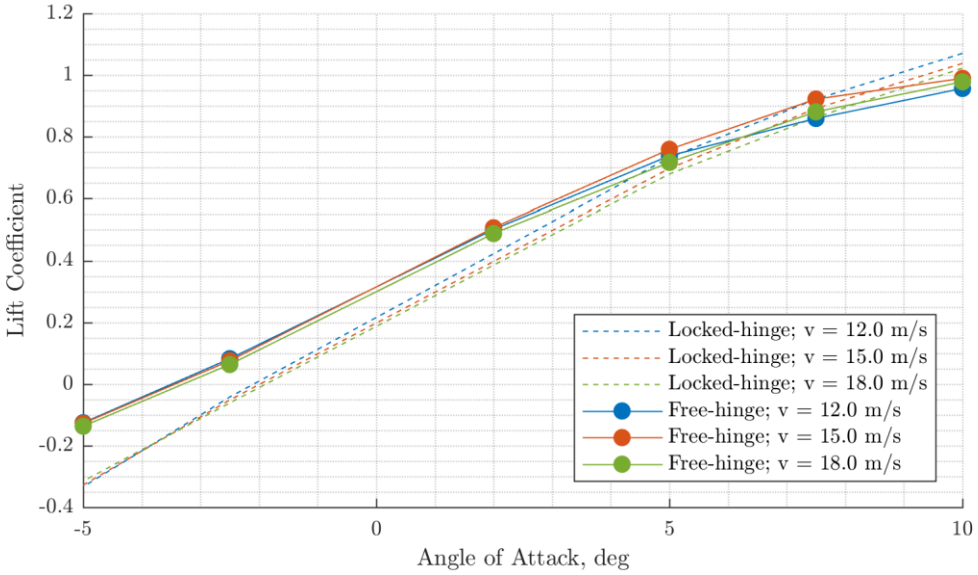

Figure 7 Variation in lift coefficient against angle of attack at wind tunnel velocity between 12.0m/s and 18.0m/s.

The reduction in the measured lift at higher angles of attack occurred because the wing had a large amount of bending deflection from the increased load and thus the normal vector of the outboard part of the wing was tilted away from the vertical. Upon considering Figure 8(a) and (b), the effect of increased bending can be seen more clearly as the lift coefficient reduces at a higher rate over increasing wind tunnel velocity than the wing-root bending moment coefficient. However, the overall lift produced in the free-hinge configuration was higher than the locked-hinge reference at negative fold angles, as shown in Figure 8(c). This is because the lift contribution from the wing-tip is more positive due to increased local angle of attack from the effect of the folding hinge geometry, as stated by Equation (1). Although the folding hinge does not transfer moments across it, the increased lift produced by the wing-tip remains carried by the hinge, and therefore the overall wing-root bending moments also became higher than the locked-hinge reference in the cases when the fold angle was negative. According to Equation (1), the change in local angle of attack is reversed at positive fold angles, which can be seen in the 5.0-deg angle of attack case at wind tunnel velocity of 22.0m/s in Figure 8, where the fold angle was positive, but the lift and the wing-root bending moment were below the locked-hinge reference. At an angle of attack of 10.0 deg and wind tunnel velocity below 16.0m/s, as well as an angle of attack of 7.5 deg and wind tunnel velocity of 12.0m/s, the lift and wing-root bending moment were also lower than the locked-hinge reference. The reduction in loads in these cases were thought to be caused by aerodynamic stall of the wing-tip, as the effect of the negative fold angle was added to the already high angle of attack.

The aero-static fold angle of the wing-tip generally increases with angle of attack and wind tunnel velocity, because the fold angle is determined by the balance of moments around the folding hinge caused by the aerodynamics and the weight of the wing-tip. In conditions when the aerodynamic drag is low and the angle of attack is small, this moment balance can be modelled as

$$qS_{WT}x_p\left(C_{L_{\alpha,WT}}(\alpha_{WT}-\alpha_{0,WT})+C_{L_{\delta,WT}}(\delta+\alpha_{WT})\right)cos\,\alpha = mgx_m\,cos\,\theta\,cos\,\alpha \tag{2}$$

where

$$\alpha_{WT} = \alpha + \Delta\alpha_{WT} \tag{3}$$

The right-hand-side of Equation (2) describes the weight moment of the wing-tip about the hinge axis, where g, m and x_m denote gravity, the mass of the wing-tip and its center of mass from the hinge axis. The left-hand-side of Equation (2) gives the aerodynamic moment about the hinge axis, where q, S_{WT} and x_p are dynamic pressure, planform area of the folding wing-tip and the distance of the pressure center of the wing-tip from the hinge axis respectively. $C_{L_{\alpha,WT}}$ denotes the lift-curve of the wing-tip and $C_{L_{\delta,WT}}$ is a function that relates lift to wing-tip tab deflection, after

accounting for its true orientation to the flow. In this simplified mathematical model, the location of the pressure center is assumed to be invariant in all conditions.

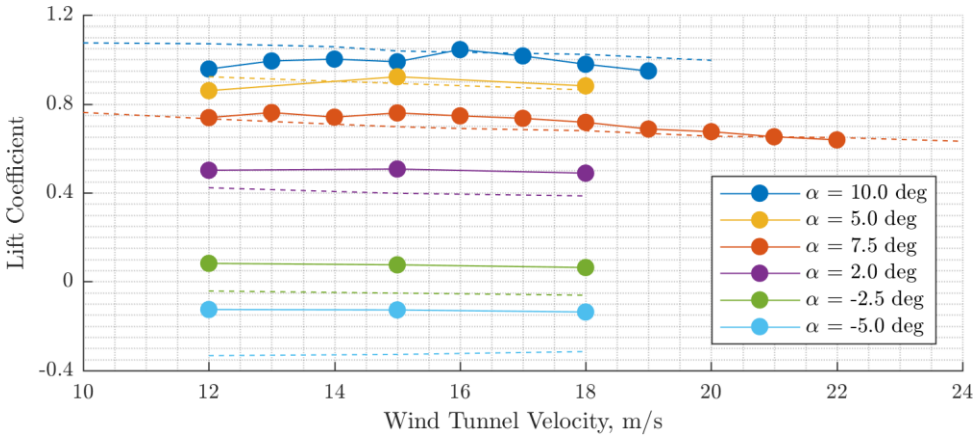

(a) Lift coefficient.

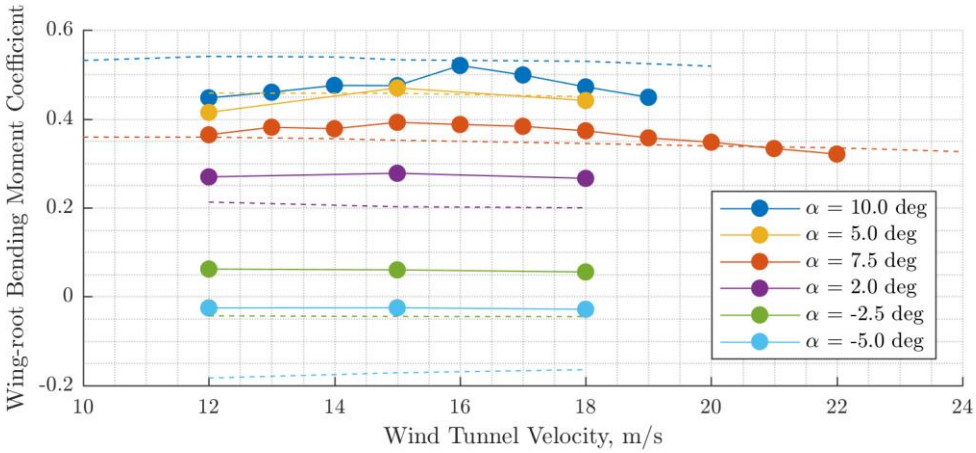

(b) Wing-root bending moment coefficient.

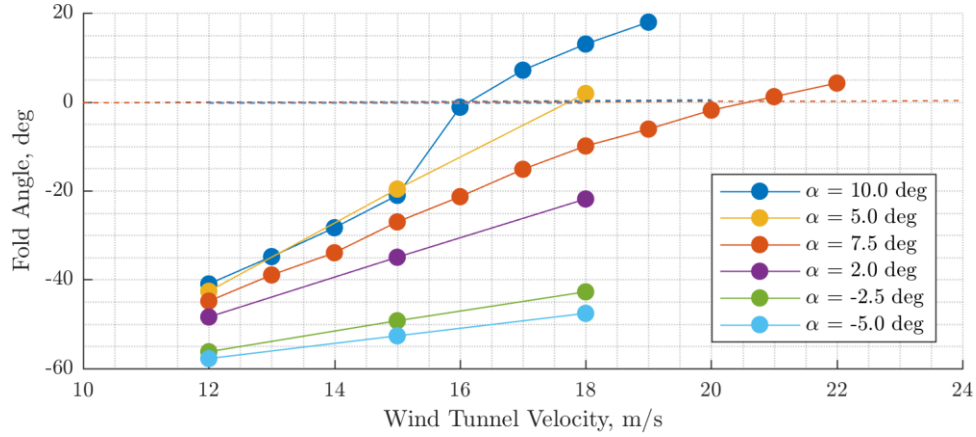

(c) Fold angle.

Figure 8 Variation against wind tunnel velocity, at angles of attack between -5.0 deg and 10.0 deg. Measurements from the locked-hinge and the free-hinge configuration are shown as dashed and solid lines respectively.

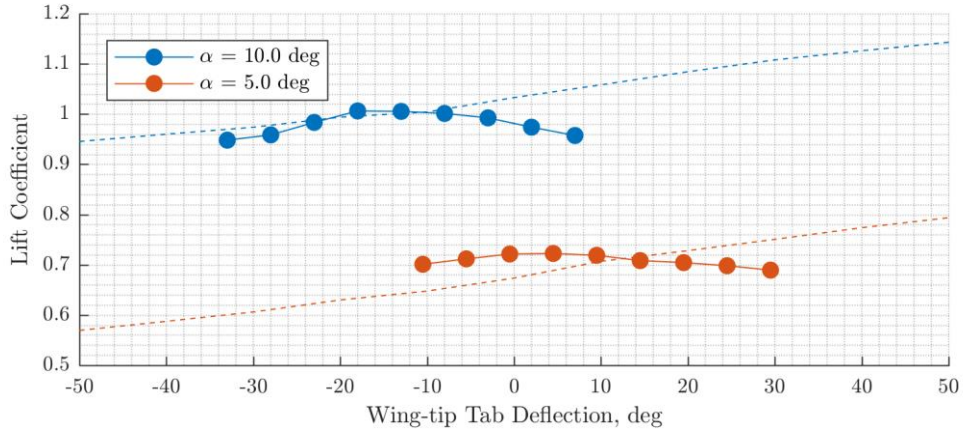

(a) Lift coefficient

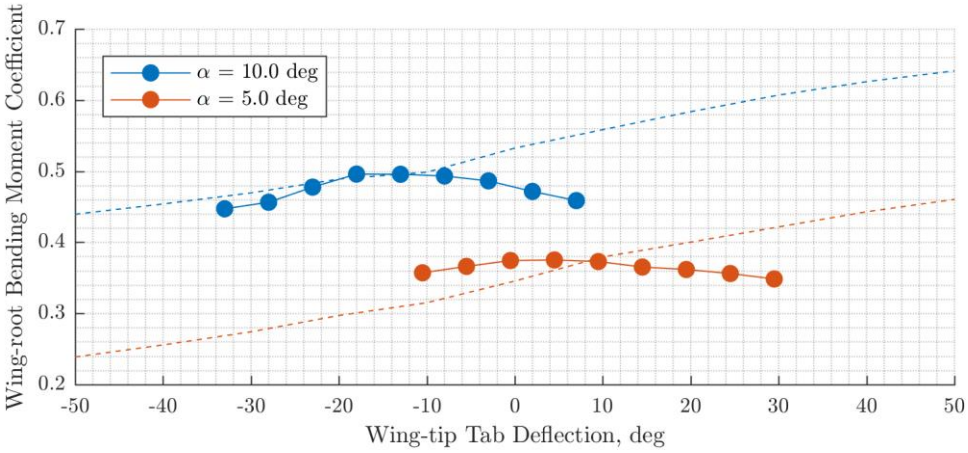

(b) Wing-root bending moment coefficient.

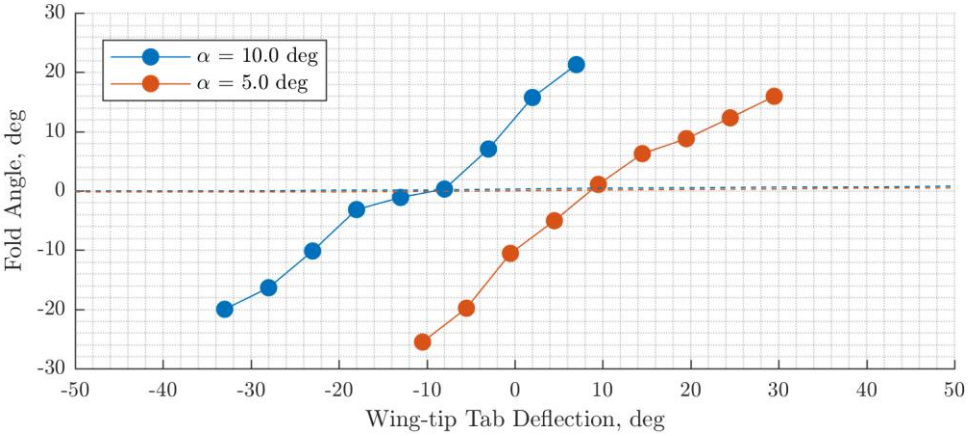

(c) Fold angle.

Figure 9 Variation against wing-tip tab deflection at angle of attack of 5.0 deg and 10.0 deg, at wind tunnel velocity of 18.0m/s. Measurements from the locked-hinge and the free-hinge configuration are shown as dashed and solid lines respectively.

Figure 9(a) and (b) show the changes in lift and wing-root bending moment against wing-tip tab deflection in the free-hinge configuration are relatively small despite the large range of fold angles, as seen in Figure 9(c). With a wing-tip tab deflection of 10.0 deg and -9.5 deg and angle of attack of 5.0 deg and 10.0 deg respectively, a fold angle of zero was achieved, i.e. the folding wing-tip was at the wing-level orientation, akin to the locked-hinge configuration.

In such condition, the measured lift was indeed similar to the locked-hinge reference, while the measured wing-root bending moment was marginally lower. This finding is an expected observation since moments are not transferred across a hinge.

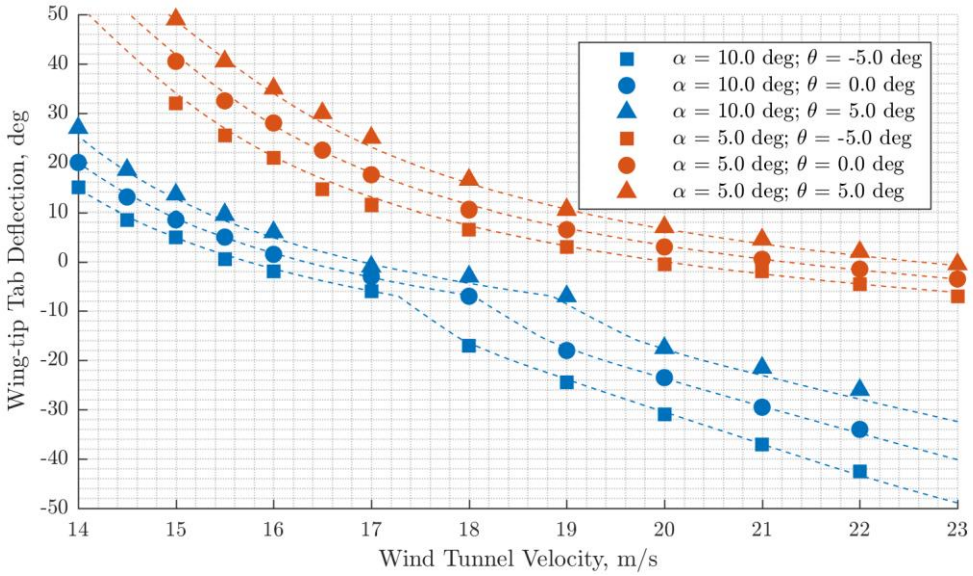

Figure 10 Relationship between fold angle and wing-tip tab deflection. Fitted results from mathematical modelling are shown as dashed lines.

The effectiveness of the wing-tip tab as a control device for aero-static fold angle is further highlighted in Figure 10, as a fold angle between -5.0 deg and 5.0 deg was achievable at angle of attack of 5.0 deg and 10.0 deg over a range of wind tunnel velocities. As expected, a more negative wing-tip tab deflection was required at higher wind tunnel velocities to counteract the otherwise increased aerodynamic moment about the hinge axis.

Table 2. Curve-fitting parameters used for wing-tip tab analysis.

S_{WT}, m^2	m, kg	x_m, m	x_p, m	$C_{L_{\alpha,WT}}$, rad^{-1}	$\alpha_{0,WT}$, rad
0.051825	0.590	0.162	0.195	2.6639	-0.0260

The fitted lines shown in Figure 10 are based on the mathematical modelling via Equation (2), using parameters listed in Table 2. The mass properties of the wing-tip were measured directly, while $C_{L_{\delta,WT}}$ and x_p were derived from the measured lift and wing-root bending moment of the locked-hinge configuration shown in Figure 9(a) and (b), and a least-squares fit was then used to determine the values for $C_{L_{\alpha,WT}}$ and $\alpha_{0,WT}$. The fitted zero-lift angle of attack shows similarity with the linearized value for the entire wing in locked-hinge configuration shown in Table 1. However, the fitted lift-curve slope of the wing-tip is significantly lower than its equivalent from the same table. This loss of lift at the wing-tip is a common phenomenon, which is linked to the formation of wing-tip vortices. Furthermore, the reduction of lift was exacerbated by the protrusion of the servo motor from the wing profile.

B. One-minus-cosine gust excitations

The gust response of the wind tunnel model was examined using a range of one-minus-cosine gust excitations at wind tunnel velocity of 18.0m/s, with the angle of attack of the wind tunnel model set to 5.0 deg. Working within the performance constraints of the gust generator, the peak deflection of the gust vanes was set to 10.0 deg, with gust lengths ranging from 1.8m to 36.0m, corresponding to 12 to 240 chord lengths. In these test cases, the wing-tip tab was deflected to the angle required for the wing-tip to achieve wing-level trim in steady-state. The deflection of the wing-tip tab remained the same throughout each gust excitation. Trimming was unnecessary for the locked-hinge configuration and therefore the wing-tip tab deflection was set to zero.

Figure 11 shows a typical gust response using the locked-hinge and the free-hinge configuration, in terms of fold angle and wing-root bending moment normalized against its steady-state value. The peak wing-root bending moment of the free-hinge configuration was substantially lower than the maximum increment from the locked-hinge reference, indicating excellent gust load alleviation performance.

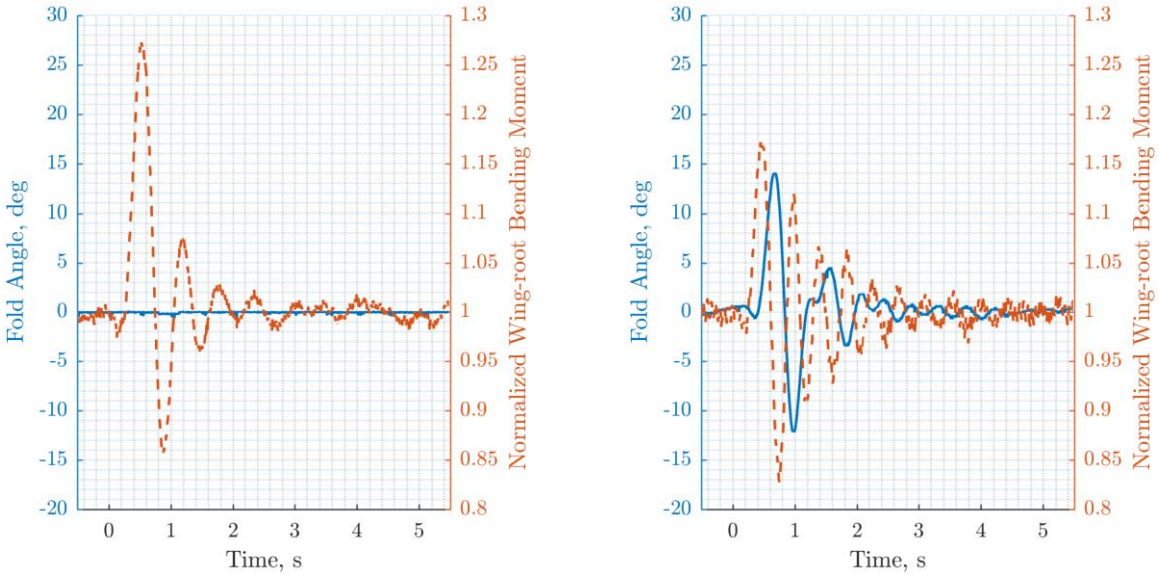

(a) Locked-hinge configuration. (b) Free-hinge configuration.

Figure 11 Response from a one-minus-cosine gust of 12.0m in length at angle of attack of 5.0 deg and wind tunnel velocity of 18.0m/s.

Figure 12 summarizes this part of the test campaign by showing the maximum and the minimum change in wing-root bending moment during one-minus-cosine gust excitations of various gust lengths. In the free-hinge configuration, the magnitude of peak wing-root bending moment was reduced compared the locked-hinge reference. However, the overall load envelope was larger and thus the minimum bending moment fell below the baseline in most of the tested conditions. The best reduction of 11% in peak load occurred at gust length of 18.0m and the advantage diminished sharply when the gust length was between 4.0m and 7.2m. The free-hinge configuration was less effective in these conditions because the effective frequency of excitation from the gust was near to the frequency of one of the wing-bending modes and caused a significant response from the inboard part of the wing. At shorter gust lengths, the folding wing-tip achieved 4% to 6% better alleviation performance in wing-root bending moment over the locked-hinge reference.

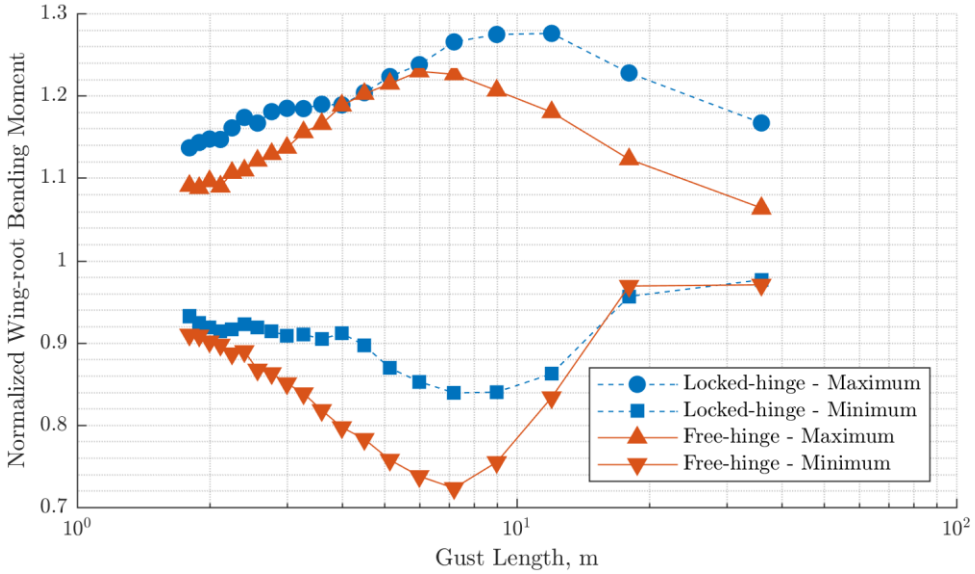

Figure 12 Load envelope of wing-root bending moment from one-minus-cosine gust excitations at angle of attack of 5.0 deg at wind tunnel velocity of 18.0m/s.

C. Prescribed wing-tip tab motion during gust encounter

This series of tests focused on using the wing-tip tab to augment positioning of the folding wing-tip during gust encounters and thus demonstrating further gains in load alleviation performance can be obtained from the use of active control. The test condition was set to an angle of attack of 5.0 deg at wind tunnel velocity of 18.0m/s, using a 7.2m one-minus-cosine gust with peak gust vane deflection of 10.0 deg. This test condition was chosen because it produced the largest load envelope and one of the highest peak wing-root bending moment amongst the previous tests.

The active control was implemented as a prescribed motion of the wing-tip tab. The deflection demand as a function of time is

$$\delta(t) = \delta_{trim} + \begin{cases} 0 & \text{for} \quad t^* \le 0 \\ \delta_p e^{-\zeta_\delta f_\delta t^*} \sin(2\pi f_\delta t^*) & \text{for} \quad 0 < t^* \le \dfrac{n_\delta}{f_\delta} \\ 0 & \text{for} \quad \dfrac{n_\delta}{f_\delta} < t^* \end{cases} \tag{4}$$

where

$$t^* = t - t_d \tag{5}$$

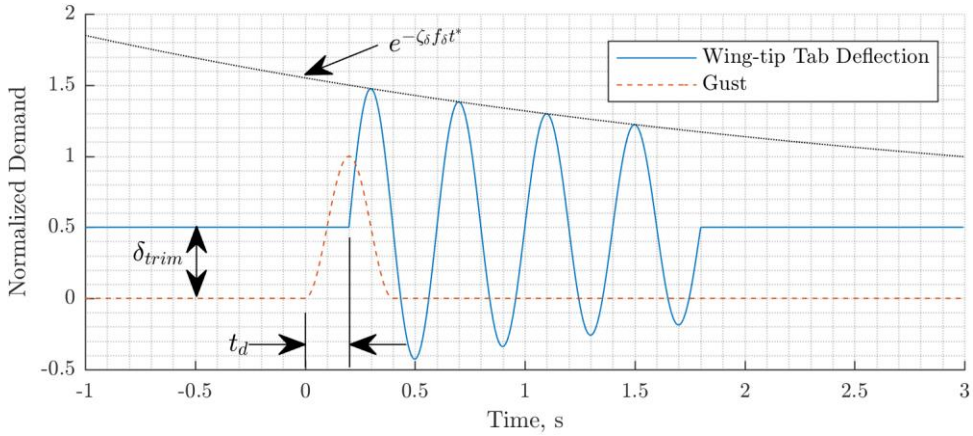

Figure 13 Timing between wing-tip tab deflection and gust generation demand.

As shown in Figure 13, t_d is a programmed delay referenced from the instant the gust vanes are triggered. At wind tunnel velocity of 18.0m/s, the time taken for the gust from triggering to arriving at the wind tunnel model was 0.2s, which meant a setting of t_d = 0.0s gave the actuation motion a head-start of 0.2s. δ_{trim} is the required deflection for maintaining the folding wing-tip at wing-level position in the steady, pre-gust condition and f_δ is the actuation frequency. For all cases, δ_p was set to 20.0 deg and n_δ was 4. This actuation scheme was chosen to boost the fold angle of the folding wing-tip during the initial phase of gust encounter, since a positive fold angle reduces the vertical load increment. In the subsequent phase of motion, deflection of the wing-tip tab then assists positioning the folding wing-tip below the wing-level orientation in order to dampen the downward motion of the inboard wing as it unloads from passing of the gust.

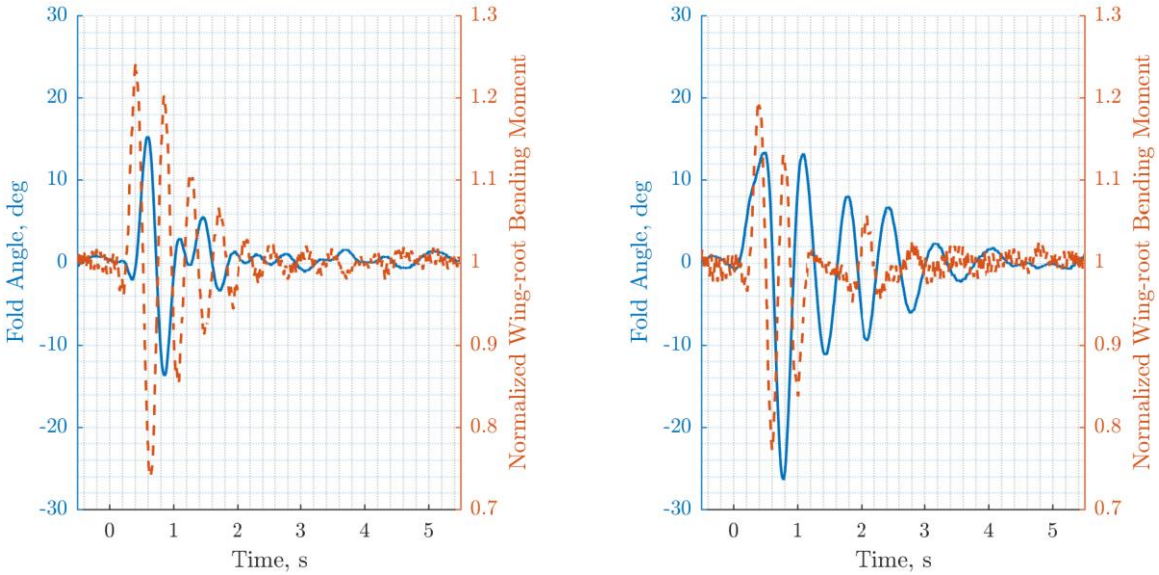

(a) No actuation.

(b) Actuation frequency of 1.5Hz, with t_d = 0.0s and ζ_δ = 0.5.

Figure 14 Response of the free-hinge configuration from a one-minus-cosine gust of 7.2m in length at angle of attack of 5.0 deg and wind tunnel velocity of 18.0m/s.

The testing began by examining the effect of actuation frequency f_δ and parameter ζ_δ have on the overall load envelope. Figure 14 provides a time-history comparison of wing-root bending moment and fold angle between the no-actuation baseline and the test case using actuation frequency of 1.5Hz, t_d = 0.0s and ζ_δ = 0.5. The peak wing-root

bending moment in the actuated case was lower, indicating further improvement in gust load alleviation performance. As shown in Figure 15, an actuation frequency of 1.5Hz generally reduced the peak wing-root bending moment as well as the size of the load envelop, with the best performance produced using ζ_δ = 0.1.

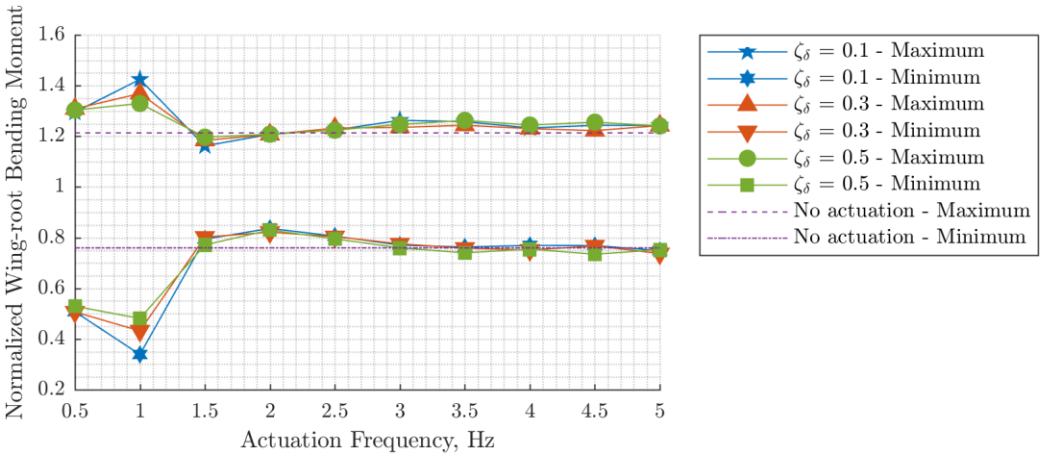

Figure 15 Variation of load envelope of wing-root bending moment from one-minus-cosine gust excitation of 7.2m in length at angle of attack of 5.0 deg and wind tunnel velocity of 18.0m/s, against actuation frequency and ζ_δ, with t_d= 0.0s.

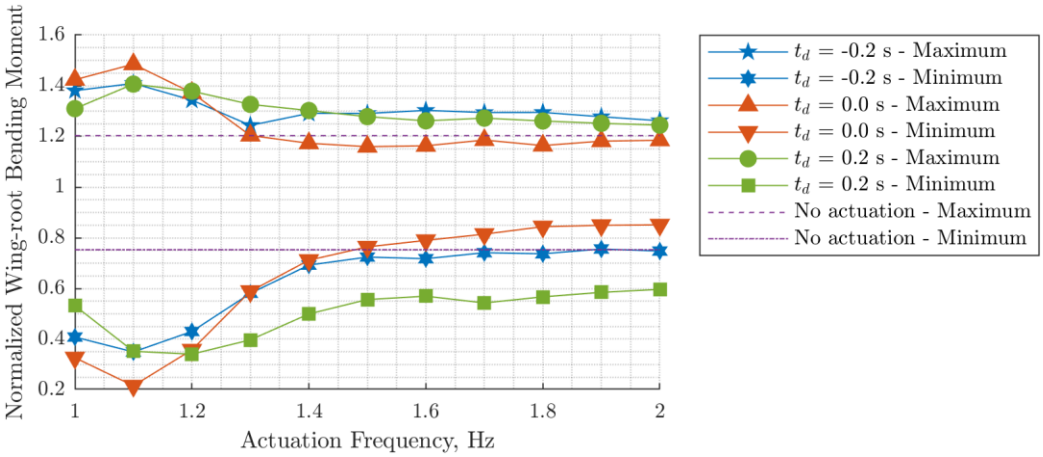

Figure 16 Variation of load envelope of wing-root bending moment from one-minus-cosine gust excitation of 7.2m in length at angle of attack of 5.0 deg and wind tunnel velocity of 18.0m/s, against actuation frequency and programmed delay, with ζ_δ = 0.1.

As shown in Figure 16, changing the programmed delay can significantly alter the overall performance of the folding wing-tip, as further reduction in the size of the load envelope from the no-actuation baseline was only possible with t_d= 0.0s and actuation frequency between 1.5Hz and 2.0Hz. Figure 17 shows the gust response in form of fold angle, wing-root bending moment and vertical acceleration of the wing measured using the accelerometer shown in Figure 5(a), with the same actuation frequency of 1.5Hz, but different programmed delays. Features in these response curves are found to be representative of cases with actuation frequency up to 2.0Hz. With t_d= -0.2s, as shown in Figure 17(a), the motion of the wing-tip tab began too early and thus the folding wing-tip was driven downwards before the peak wing-root bending moment occurred, therefore the achievable load alleviation was limited. Figure 17 (b) shows t_d= 0.0s is an excellent setting for further gains in load alleviation. During the initial phase of vertical acceleration caused by the gust, the wing-tip was already in a raised position due to deflection of the wing-tip tab, which limited the peak wing-root bending moment as intended. The subsequent downward movement of the folding wing-tip also coincided with post-gust unloading of the inboard wing, as indicated by its downward acceleration, which dampened the overall motion and reduced the size of the load envelope. As shown in Figure 17(c), with t_d=

0.2s, the delay was too long such that positioning of the folding wing-tip became in-phase with the vertical acceleration of the inboard wing, which in fact increased the magnitude of wing-root bending moment at certain phase of the gust response.

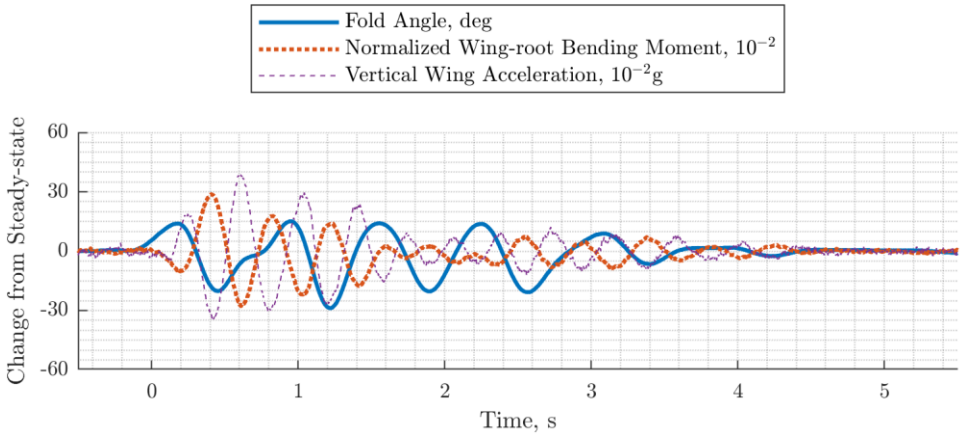

(a) t_d= -0.2s

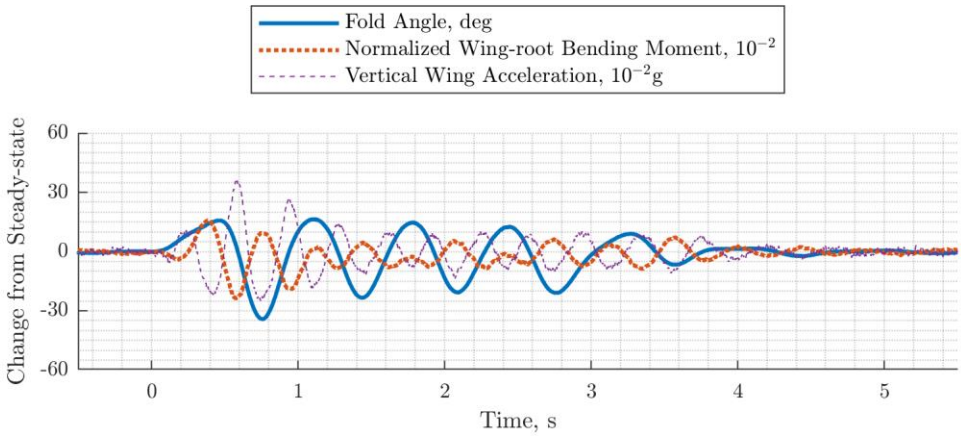

(b) t_d= 0.0s

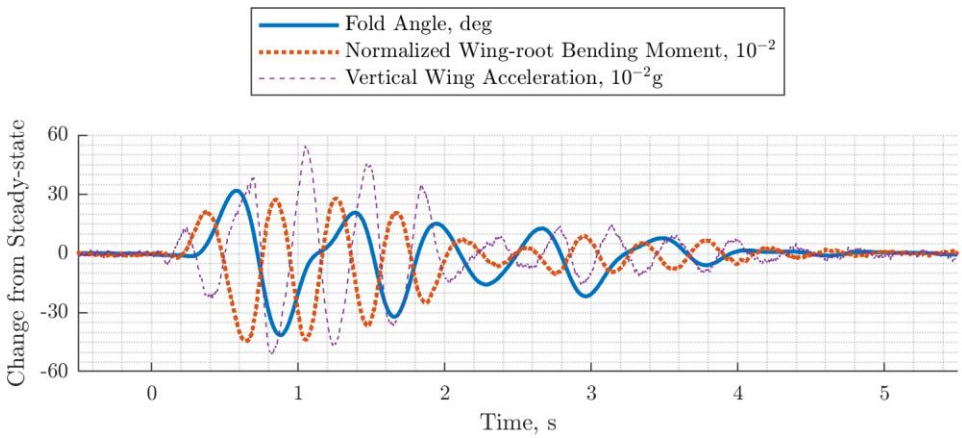

(c) t_d= 0.2s

Figure 17 Response from a one-minus-cosine gust of 7.2m in length at angle of attack of 5.0 deg and wind tunnel velocity of 18.0m/s, with actuation frequency set to 1.5Hz, ζ_δ = 0.1, and varying programmed delay.

IV. Conclusions

Low-speed wind tunnel testing was conducted using a flexible, high aspect ratio wing fitted with a folding wing-tip, of which the folding hinge axis was orientated 10.0 deg from the flow direction. In steady conditions, the behavior of the folding wing-tip was found to be consistent with observations made from previous studies, despite the increase in flexibility of the inboard wing. Gust excitations based on the one-minus-cosine profile were carried out to assess the gust loads alleviation performance of the folding wing-tip concept and found that the folding wing-tip was effective at reducing the peak positive increment in wing-root bending moment, achieving 6% reduction against the locked-hinge, non-folding baseline in shorter gust lengths and 11% when the gust lengths became longer. However, the load envelope during the gust encounter became larger in some conditions, meaning the lowest wing-root bending moment fell below the locked-hinge reference.

The folding wing-tip was additionally fitted with a movable secondary aerodynamic surface intending for controlling the folding action of the wing-tip through aerodynamic means. It was demonstrated in the steady aerodynamic tests that such a device was able to maintain the orientation of the wing-tip over a range of wind tunnel velocities and angles of attack, including trimming the folding wing-tip to the wing-level position. It was also shown in the gust excitation tests that actuating the secondary aerodynamic surface with a suitable timing in relation to the arrival of the gust could further reduce the peak wing-root bending moment and the size of the overall load envelope, thus improve upon the level of gust load alleviation already achieved by the folding wing-tip alone. Further work is ongoing, including implementation of a closed-loop control system.

References

[1]Lassen M.A., D. C. R., Jones K.T. and Kenning T.B., "Wing fold controller", U.S. Patent Application No. 14/022,622, Publication No. US20140014768A1, Jan. 16, 2014

[2]Jutte, C. D. R. a. C. V., "Survey of Applications of Active Control Technology for Gust Alleviation and New Challenges for Lighter-weight Aircraft",NASA/TM—2012–216008, 2012

[3]Cheung, R., Rezgui, D., Cooper, J., and Wilson, T. "Testing of a hinged wing-tip device for gust loads alleviation," *Journal of Aircraft*, 2018.doi: 10.2514/1.C034811

[4]Castrichini, A., Siddaramaiah, V. H., Calderon, D. E., Cooper, J. E., Wilson, T., and Lemmens, Y. "Preliminary investigation of use of flexible folding wing tips for static and dynamic load alleviation," *The Aeronautical Journal* Vol. 121, No. 1235, 2017, pp. 73-94.doi: 10.1017/aer.2016.108

[5]Wilson, T., Castrichini, A., Azabal, A., Cooper, J. E., Ajaj, R., and Herring, M. "Aeroelastic Behaviour of Hinged Wing Tips," *International Forum on Aeroelasticity and Structural Dynamics*. Como, Italy, 2017.

[6]Cheung, R. C. M., Castrichini, A., Rezgui, D., Cooper, J. E., and Wilson, T. "Wind Tunnel Testing of Folding Wing-Tip Devices for Gust Loads Alleviation," *International Forum on Aeroelasticity and Structural Dynamics*. Como, Italy, 2017.

[7]Castrichini, A., Hodigere Siddaramaiah, V., Calderon, D. E., Cooper, J. E., Wilson, T., and Lemmens, Y. "Nonlinear Folding Wing Tips for Gust Loads Alleviation," *Journal of Aircraft* Vol. 53, No. 5, 2016, pp. 1391-1399.doi: 10.2514/1.C033474

[8]Castrichini, A., Cooper, J. E., Wilson, T., Carrella, A., and Lemmens, Y. "Nonlinear Negative Stiffness Wingtip Spring Device for Gust Loads Alleviation," *Journal of Aircraft* Vol. 54, No. 2, 2016, pp. 627-641.doi: 10.2514/1.C033887

[9]Gatto, A., Mattioni, F., and Friswell, M. I. "Experimental Investigation of Bistable Winglets to Enhance Aircraft Wing Lift Takeoff Capability," *Journal of Aircraft* Vol. 46, No. 2, 2009, pp. 647-655.doi: 10.2514/1.39614

[10]Wood, K. T., Cheung, R. C., Richardson, T. S., Cooper, J. E., Darbyshire, O., and Warsop, C. "A New Gust Generator for a Low Speed Wind Tunnel: Design and Commissioning," *55th AIAA Aerospace Sciences Meeting*. American Institute of Aeronautics and Astronautics, 2017.